Mechanical and Tribological Properties of CrWN/MoN Nano-Multilayer Coatings Deposited by Cathodic Arc Ion Plating

Canxin Tian [1,*], Yanxiong Xiang [1], Changwei Zou [1], Yunjiang Yu [1], Tushagu Abudouwufu [2,3], Bing Yang [4] and Dejun Fu [2,5,*]

1   School of Physical Science and Technology, Lingnan Normal University, Zhanjiang 524048, China
2   School of Physics and Technology, Wuhan University, Wuhan 430072, China
3   Zhuhai Tsinghua University Research Institute Innovation Center, Zhuhai 519000, China
4   School of Power & Mechanical Engineering, Wuhan University, Wuhan 430072, China
5   Wuhan University Shenzhen Research Institute, Nanshan Hitech Zone, Shenzhen 518057, China
*   Correspondence: cxtian@lingnan.edu.cn (C.T.); djfu@whu.edu.cn (D.F.)

Abstract: CrWN/MoN nano-multilayer coatings were deposited in pure N_2 by multi-arc ion plating using CrW and Mo targets, with the cathode co-controlled by a permanent magnet combined with an electromagnet. The effects of the thickness modulation period on the microstructure and mechanical and tribological performance were systematically analyzed by grazing-incident X-ray diffraction (GIXRD), transmission electron microscopy (TEM), Nanoindentation, scanning electron microscope (SEM) and profilometry using a Talysurf profilometer. The local coherent interfaces and nanoscale modulation period were confirmed by TEM, while the coatings were confirmed to be composed of fcc-CrWN and hexagonal δ-MoN by GIXRD. With the increase in the modulation period, the hardness of the CrWN/MoN nano-multilayer coatings decreased, and the values of the H/E ratio and friction coefficient showed the same variation trend. At an 8.0 nm modulation period, the CrWN/MoN nano-multilayer coating showed the maximum hardness (30.2 GPa), the lowest H/E value (0.082) and an H^3/E^{*2} value of 0.16. With the decrease in the modulation period, the average friction coefficient of the CrWN/MoN nano-multilayer coatings gradually decreased from 0.45 to 0.29, while the wear rate decreased from 4.2×10^{-7} mm^3/Nm to 3.3×10^{-7} mm^3/Nm.

Keywords: CrWN/MoN nano-multilayer coatings; multi-arc ion plating; thickness modulation period; mechanical properties; tribological properties

1. Introduction

Transition metal nitrides, exhibiting high hardness and wear, corrosion and oxidation resistance, have been widely used for surface strengthening in the past decades. Among them, CrN coatings are widely used in wear components, molding dies and cutting tools due to their low internal stress. However, it has some limitations that hardly overcomes modern challenges. For example, the relatively low hardness and high friction coefficient can lead to the premature failure of CrN coatings. Yao et al. [1] found that the hardness and wear resistance of CrN coatings can be improved by adding W. Compared with CrN coatings, the Knoop hardness of CrWN was increased by HK 1000, while the wear resistance was improved by 85%. Jasempoor et al. [2] studied the mechanical, tribological and electrochemical behaviors of CrN monolayer and Cr/CrN multilayer coatings. The hardness of CrN monolayer and Cr/CrN multilayer coatings was 21.5 and 23.3 GPa, while the friction coefficients were 0.61 and 0.46, respectively. The corrosion resistance of Cr/CrN multilayer coatings was higher than that of CrN single-layer coatings, which could be ascribed to a multilayer architecture. These studies show that alloying and multilayer structuring can improve the properties of CrN coatings.

Alloying is the addition of new elements to an existing coating to meet the requirements of specific applications. In a review, Hauert [3] explained that a new single-phase

coating or a biphasic coating can be produced by adding new elements to existing coatings. For example, Ding [4] and Endrino [5] tried to improve the hardness, oxidation resistance and wear resistance of CrN coatings by adding Al, while Lin et al. [6] added Si to CrN coatings. They found that the hardness and oxidation resistance could be improved when the CrAlN coatings kept the cubic phase structure [4,5]. The incorporation of smaller Al atoms into the lattice of CrN leads to local tensile stress, which contributes to the higher hardness. Because of the formation of oxides and oxynitrides on the surfaces of CrAlN coatings, the oxidation resistance of AlCrN coatings is increased [5]. Lin et al. [6] prepared nanocrystalline–amorphous composite biphasic coatings of nc-CrN/a-Si$_3$N$_4$ by adding metalloid Si to CrN. The improved hardness, wear resistance and corrosion resistance are mainly attributed to the nanocomposite structure. The strengthened interfaces play a critical role [6].

A multilayer architecture consisting of two or more different material layers can combine the advantages of the constituent layers [7,8]. Owing to the fact that the propagation of cracks and dislocations can be blocked or stopped at the interfaces or in the ductile material layer, multilayer coatings show better performance [9,10]. Especially the nanoscale multilayered structure coatings, combining Hall–Petch strengthening [11], the superlattice effect [12] and supermodulus effects [13], the properties of the multilayer coatings can be additionally improved [14]. Helmersson et al. [15] found that the maximum hardness of TiN/VN nano-multilayer coatings is larger than 50 GPa when the modulation period (Λ) is in the range of 5–10 nm. Kim et al. [16] demonstrated that the interface structure plays a key role in the hardness enhancement of TiN/VN nano-multilayer coatings. No supermodulus effect is shown in the TiN/VN nano-multilayer coatings, and the shear moduli of the TiN and VN layers are different [16].

The aim of alloying and multilayer coatings is to create new properties from the combination of suitable materials and microstructures. From the research of Hones [17] and Yau [18], it can be seen that W-doped CrN films with a blend of solution strengthening and changes in chemical bonding exhibit excellent hardness, adhesion and mechanical properties that help resist wear damage. Lin et al. [19] studied the mechanical properties and oxidation resistance of (Cr,W) N coatings and demonstrated that CrWN coatings with low tungsten content exhibited excellent hardness and oxidation resistance. Tungsten is considered to be one of the most effective alloying elements [19]. Researchers have reported that binary transition metal nitride Mo-N coatings exhibit a low friction coefficient due to the formation of self-lubricating Magnéli phase MoO$_3$ [20–22]. As reported in the literature, Postolnyi et al. [23] designed multilayer CrN/MoN coatings and concluded that the mechanical and tribological properties of CrN/MoN coatings can be improved by a multilayer architecture, which benefits from the synergistic effect of individual layer properties, as well as Hall–Petch strengthening and the superlattice effect. Pogrebnjak et al. [24] found similar results in their study of CrN/MoN coatings. Thus, the synergy caused by both W-alloyed CrN and MoN layers can make nano-multilayered CrWN/MoN coatings promising materials with enhanced mechanical and tribological performance.

In this paper, CrWN/MoN nano-multilayer coatings with different modulation periods (Λ) were prepared in pure N$_2$ by cathodic arc ion plating using CrW and Mo targets, with the cathode co-controlled by a permanent magnet and an electromagnet. The aim of this investigation was to determine the effects of the nano-period Λ on the structure and mechanical and tribological properties of CrWN/MoN nanocomposite coatings and obtain good nano-multilayer CrWN/MoN coatings with the potential for industrial production.

2. Experimental Details

CrWN/MoN coatings with various modulation periods (Λ) were deposited on polished substrates of cemented carbide by arc ion plating using CrW and Mo targets. The substrates were ultrasonically cleaned in acetone, alcohol and deionized water sequentially. After drying in hot air, the substrates were clamped to the holder of a vacuum chamber. The distance was 250 mm from the substrates to the cathodic source. The purity of Ar and N$_2$ gases was 99.999%, and that of the Mo and CrW (95:5 at.%) targets was 99.6%. The coating

includes the pure Mo metal layer, the MoN layer and the CrWN/MoN nano-multilayers. The preparation parameters of CrWN/MoN coatings are shown in Table 1. The rotation speed of the substrates was controlled between 0.5 rpm and 3 rpm, which makes it easier to obtain much different Λ. The thickness ratio of the MoN and CrWN layers is around 2.5:1 for the nano-multilayer structure.

**Table 1.** Deposition parameters of the CrWN/MoN nano-multilayer coatings.

Deposition Parameter	Values
Bias voltage/V	−120
Target material	CrW (95:5 at.%), Mo
Deposition pressure/Pa	1.0
Target current/A	CrW (80), Mo (125)
Temperature/°C	400
Reaction gas	N_2
Substrates rotation speeds/(rpm)	0.5, 1, 2, 3
Target substrate distance/mm	250
Deposition time/min	180

The crystal structures of the CrWN/MoN coatings were characterized by grazing-incident X-ray diffraction (Smart Lab X, Rigaku, Japan). The surfaces and cross-sections of the coatings were examined by field-emission scanning electron microscopy (Nova Nano 430, FEI, Hillsboro, OR, USA). The detailed microstructures were studied by high-resolution transmission electron microscopy (HRTEM) using an Tecnai G2 F20 S-TWIN (FEI, Hillsboro, OR, USA). The hardness and elastic moduli of the coatings were measured by an Agilent NanoIndenter G200 hardness tester (CSM, Peuseux, Switzerland) under a load of 30 mN. Six points were measured and averaged for each sample. The friction coefficients (COFs) of the coatings were tested by UMT-Tribo lab friction tester (Bruker, Billerica, MA, USA) in ambient air, with a temperature of 30 °C and a relative humidity (RH) of 80%; in order to determine the wear rates of the CrWN/MoN coatings, a Si_3N_4 ball (6 mm in diameter) was used as the mating material and a load of 15 N was applied on the ball. The sliding speed of the friction pair was 0.04 m/s. The COF was recorded during the tests. The wear rate (Wr) was calculated from the groove dimensions determined by a TALYSURF CLI 1000 Profiler (Taylor Hopson, Leicester, UK).

3. Results and Discussion

The XRD patterns of CrWN/MoN nano-multilayer coatings with different Λ (see the TEM results) and the peak positions of monolayer fcc-CrWN and hexagonal δ-MoN coatings are presented in Figure 1a, and the corresponding grain sizes of the multilayer and monolayer coatings are shown in Figure 1b. The CrWN/MoN coatings show a biphasic structure of fcc-CrWN and hexagonal δ-MoN. The diffraction peaks of CrWN/MoN coatings locates between the fcc-CrWN and hexagonal δ-MoN. When Λ is 45 nm and 25 nm, one can see the diffraction peaks of fcc-CrWN and hexagonal δ-MoN. When Λ decreases to 13 nm and 8 nm, the peaks of δ-MoN (202) and (222) disappear, as well as those of fcc-CrWN (220) and (311), which coincides with the TEM ring analysis for the same coating. As Λ decreases, the intensity of the diffraction peaks of the CrWN/MoN nano-multilayer coatings gradually decreases, and the peak of CrWN/MoN coatings near 36.5° shifts from the (200) peak of monolayer δ-MoN at 35.8° to the peak (111) of monolayer CrWN at 37°, which indicates possible structural and stress evolution in the layers of the coatings [25]. The crystallite size is estimated by the Debye–Scherrer formula [18]. The crystallite size of CrWN monolayer coatings is about 11–12 nm, while the values of MoN monolayer coatings are about 7–8 nm. With decreasing Λ, the grain size of CrWN/MoN nano-multilayer coatings decreases from 4–5 nm to 1.5 nm, which is lower than the size of monolayer CrWN and δ-MoN grains, as shown in Figure 1b. With decreasing Λ, the

nano-multilayer structure shows broadened diffraction peaks, which means that the grains of CrWN/MoN coatings are inhibited [26].
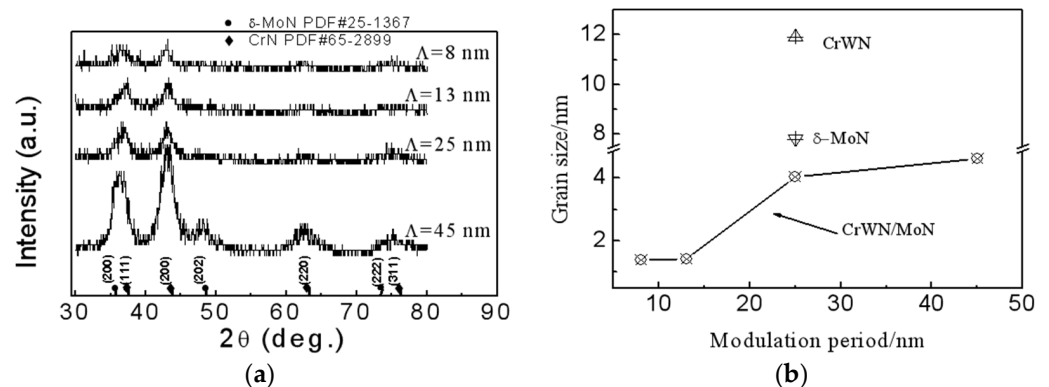
Figure 1. XRD patterns (**a**) and grain sizes (**b**) of the CrWN/MoN nano-multilayer coatings with different modulation periods and monolayer CrWN and δ-MoN coatings.

From the present experiment, one cannot see obvious differences in the surface morphologies of the CrWN/MoN nano-multilayer coatings with the variation in Λ. Figure 2 shows the typical surface and cross-sectional SEM morphology of the CrWN/MoN nano-multilayer coating with Λ = 13 nm. Macro-particles and pit holes are observed on the surface of the coating, while a dense structure can be seen in the cross-sectional image. The thickness of the samples is about 3.5 μm. Compared with nitride coatings prepared by permanent-magnet arc ion plating [27–29], large particles are effectively inhibited on CrWN/MoN nano-multilayer coatings prepared by permanent magnet and electromagnetic co-controlled arc ion plating technology. The combination of the electromagnet and permanent magnet can optimize the magnetic field on the surface of the cathode. The optimized magnetic field can accelerate the arc motion and avoid overheating the cathode spots, which are otherwise located in one position, which effectively inhibits the eruption of large melt droplets [30,31]. The number of large particles on the coatings does not increase, even with 125 A as the Mo target current. The melting point of Mo is 2468 °C. The high melting point is one factor preventing the formation of droplets on the CrWN/MoN nano-multilayer coatings [32]. Contrary to the Mo cathode, which is difficult to run stably in conventional arc ion plating, the Mo target co-controlled by the permanent magnet and electromagnet runs more stably.
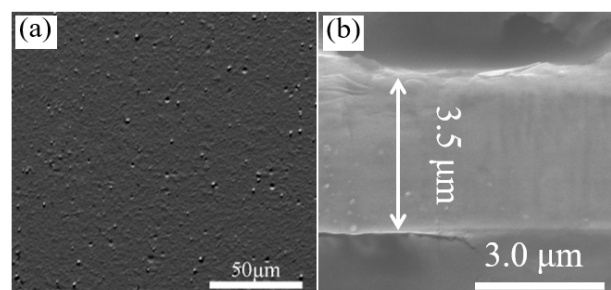
Figure 2. Surface (**a**) and cross-sectional (**b**) SEM images of the CrWN/MoN nano-multilayer coating with Λ = 13 nm.

The TEM cross-sections and corresponding selection electron diffraction of CrWN/MoN coatings are shown in Figure 3. No obvious penetrating columnar crystals can be seen in the TEM micrographs. One sees clear nano-multilayered structures, with bright CrWN layers alternating with dark δ-MoN layers. The calculated Λ values of the coatings are about 45 nm, 25 nm, 13 nm and 8 nm. The interface is fuzzy and non-smooth between the fcc-CrWN and δ-MoN layers. For the CrWN/MoN coating with Λ = 45 nm, one thin black interlayer can be

seen in the white CrWN layer. According to reference [33], the thin black layer is the δ-MoN layer and is caused by the two-dimensional rotation of the sample holder. The nano-multilayer structure of the coatings is obtained by adjusting the rotation speed of the substrates. Blend of the lower rotation speed and higher Mo target current (125 A), the substrates rotated to the front of the CrW target are coated by the Mo target at one certain time. With increasing rotation speed, the interlayer becomes less obvious. This kind of mixing may be one reason for the unstable properties of nano-layered coatings. For example, the superlattice effect is easily lost if the layer constituents of the multilayer coating do not match [34]. Selected-area electron diffraction (Figure 3 inset) confirms the existence of mixed fcc-CrWN and hexagonal δ-MoN phases, which is consistent with the results of XRD. One of the diffraction rings of all samples is observed to correspond to fcc-CrWN (111) or δ-MoN (200), a phenomenon consistent with the XRD data, which show little difference in the lattice parameters of fcc-CrWN (111) and δ-MoN (200). The other diffraction rings of the samples with 45 nm and 25 nm Λ are observed to correspond to fcc-CrWN (200) and (220) and δ-MoN (202), while only fcc-CrWN (200) is observed for the samples with 13 nm and 8 nm Λ. The positions and structures of the diffraction rings accord well with the XRD data. The smaller lattice difference between fcc-CrWN (111) and δ-MoN (200) is more likely to enable coherent growth [14]. The CrWN/MoN nano-multilayer exhibits the possibility of forming a coherent interface.
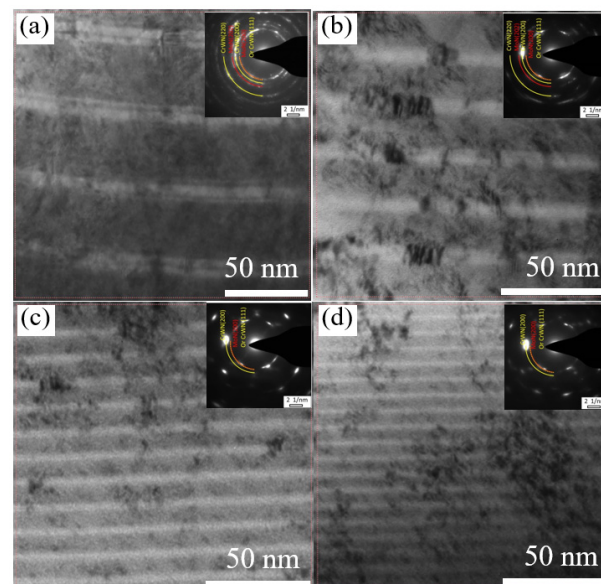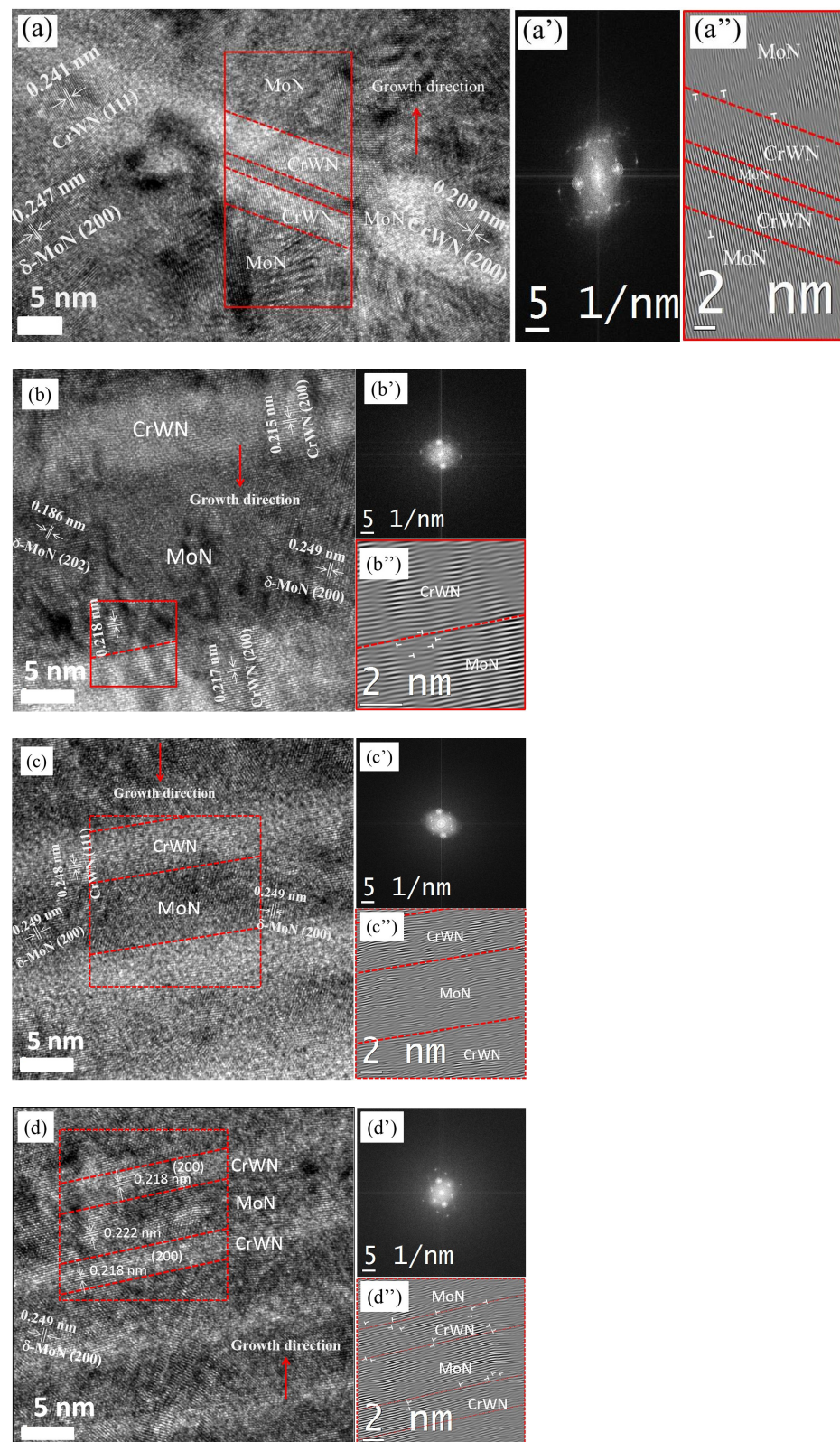

Figure 3. Cross-sectional TEM images and corresponding selection electron diffraction pattern of the CrWN/MoN nano-multilayer coatings with different modulation periods: (**a**) 45 nm, (**b**) 25 nm, (**c**) 13 nm, (**d**) 8 nm.

To investigate the CrWN/MoN nano-multilayer coatings in more detail, a high-resolution transmission electron micrograph (HRTEM) analysis was performed, as shown in Figure 4. One sees the fuzzy interfaces of nano-multilayer coatings. With the variation in Λ, the interface is clearly changed. Further detailed studies show that the CrWN/MoN nano-multilayer coatings have coherent interfaces in a few regions. Figure 4a shows the HRTEM micrograph of the CrWN/MoN coating with Λ = 45 nm. The rectangular region outlined in Figure 4a shows that continuous lattice fringes run through the entire CrWN layer and extend into the δ-MoN layers. One can see the epitaxial interface and edge dislocation between the CrWN and MoN layers from the fast Fourier transformation (FFT) and inverse fast Fourier transformation (IFFT) images in Figure 4a′,a″. The minimization of the total energy of coherent strain energy and interfacial energy is believed to be the driving force for the formation of coherent interfacial energy. A coherent interface of a multilayer can be obtained when the coherent interface energy is higher than the coherent strain energy [17,23]. Additionally, the dislocation at the interfaces of the CrWN and MoN layers, as shown in Figure 4a″, can reduce the coherent strain

and improve the local stability of coherent interfaces. The thin MoN interlayer in the CrWN layer is an overall epitaxial structure with CrWN, and the thickness of the thin MoN layer is 1.5 nm. In references [35,36], it was revealed that one material may act as a template and force a thin enough layer of another material into its own crystallographic structure, such as TiN/AlN superlattice coatings, where the crystal structure of AlN changes from the hexagonal type to the TiN NaCl type for superlattice periods smaller than 3 nm. The HRTEM micrographs of the CrWN/MoN coatings with 25 nm, 13 nm and 8 nm are shown in Figure 4b–d, where no penetrating lattice fringe (as shown in Figure 4a) is observed in the interface. From the IFFT images in Figure 4b″,d″, one can see the obvious localized coherent interfaces and an edge dislocation between the CrWN and MoN layers. As shown in Figure 4c″, the formation of coherent interfaces is not observed in the CrWN/MoN coating with 13 nm Λ. The reason may be that the coherent strain energy is higher than the coherent interface energy. Several grains in the CrWN and δ-MoN layers with different growth orientations, CrWN (111), (200), and δ-MoN (200), (202), are observed in Figure 4, which may reduce the strain energy, similar to the renucleation of CrWN and δ-MoN [37]. The small grain size in the nanolayer means that grain growth is blocked, which is consistent with the XRD results, as shown in Figure 1.

Figure 5 shows the hardness and elastic modulus of the CrWN/MoN nano-multilayer coatings with different Λ; the inset is the hardness and elastic modulus of the 25 nm Λ coating with displacement into its surface. With the displacement into 300 nm of surface, the hardness of the coating is about 29.6 Gpa while the elastic modulus is about 296.6 Gpa. With increasing Λ, the hardness of CrWN/MoN nano-multilayer coatings decreases from 30.2 GPa to 25.5 GPa and then increases to 29.5 GPa. In our previous studies, the hardness of CrN, CrWN and δ-MoN prepared by cathodic arc plating were 16–18 GPa [38], 19–20 GPa [39] and 20–21 GPa [38], respectively. The hardness of the CrWN/MoN nano-multilayer coatings reaches 30 GPa, which is also higher than that of the conventional monolayer TiN [40] and ZrN [41] coatings. This hardness enhancement of the CrWN/MoN nano-multilayer is mainly dependent on the nano-multilayer microstructure. Correspondingly, the Λ variation in the nano-multilayer leads to a similar variation trend of the elastic modulus. According to the sectional morphologies of the CrWN/MoN nano-multilayer coatings, as shown in Figure 2 (SEM) and Figure 3 (TEM), no obvious columnar crystals can be seen in the coatings. Therefore, the multilayer structure effectively inhibits the generation of columnar crystal structure and obtains the dense microstructure which is positive on hardness [42]. In addition, the growth of nanoscale grains can result in a significant hardness enhancement [43]. As shown in Figure 1b, with the decrease in Λ, the grain size decreases, which is useful for increasing the hardness of CrWN/MoN nano-multilayer coatings according to the Hall–Petch relationship [44]. As a result, the CrWN/MoN nano-multilayer coating with Λ = 8 nm has the maximum hardness and elastic modulus. However, the CrWN/MoN coating with 13 nm Λ has the minimum hardness, which can be attributed to interfacial structural changes, such as incoherent interfaces, as shown in Figure 4c″. In reference [45], Chen et al. observed that the hardness of CrAlN/TiN multilayer coatings with coherent interfaces and local coherent interfaces was higher than that of coatings with incoherent interfaces. Yalamanchili et al. observed that the hardness of TiN/ZrAlN multilayers with semicoherent interfaces was higher than that of coatings with incoherent interfaces [46]. As barriers to dislocation movement, the defects at interface boundaries and the coherency strain of the multilayer coatings are useful for hardness enhancement [47].
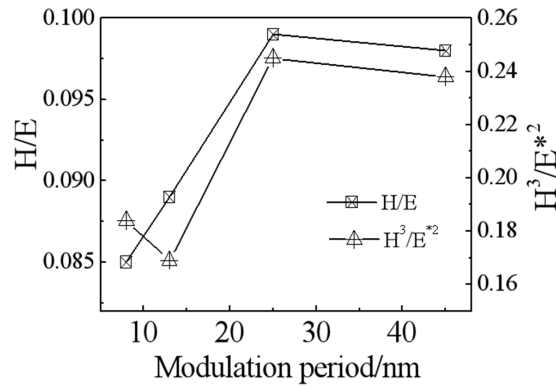
Figure 6 shows the calculated H/E and H^3/E^{*2} ratios of CrWN/MoN nano-multilayer coatings at Λ values ranging from 8 nm to 45 nm, and H is the hardness of the coating, E is the elastic modulus, effective elastic modulus $E^* = E/(1 - v^2)$, v is Poisson's ratio 0.29. With increasing Λ, the H/E ratio of the CrWN/MoN nano-multilayer coatings increases from 0.078 to 0.09, while the H^3/E^{*2} ratio decreases from 0.184 to 0.169, followed by an increase to 0.24. H/E follows a similar evolutionary trend to that of the COF and wear rate, as shown in Figure 7. Research shows that H/E and H^3/E^{*2} are related to the toughness of hard coatings [48]. H/E is correlated to resistance to the elastic strain failure of the coatings, while H^3/E^{*2} is related to the resistance to plastic deformation [49–51].

Figure 4. Cross-sectional HRTEM images of the CrWN/MoN nano-multilayer coatings with different modulation periods: (**a**) 45 nm, (**b**) 25 nm, (**c**) 13 nm, (**d**) 8 nm. (**a'**) The FFT pattern for the marked area in (**a**). (**a''**) The corresponding IFFT image in (**a'**). (**b'**) The FFT pattern for the marked area in (**b**). (**b''**) The corresponding IFFT image in (**b'**). (**c'**) The FFT pattern for the marked area in (**c**). (**c''**) The corresponding IFFT image in (**c'**). (**d'**) The FFT pattern for the marked area in (**d**). (**d''**) The corresponding IFFT image in (**d'**).
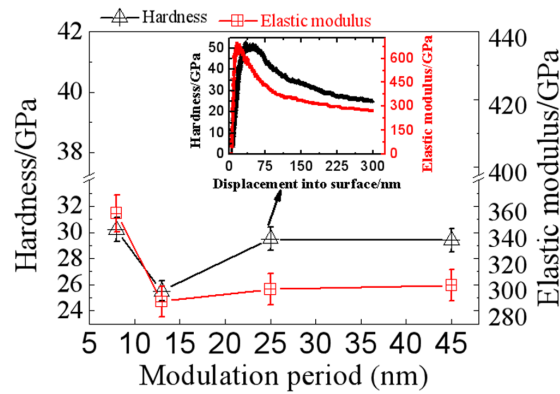
Figure 5. The hardness and elastic modulus of the CrWN/MoN nano-multilayer coatings with different modulation periods. The inset is the hardness and elastic modulus of the 25 nm Λ coating with displacement into its surface.
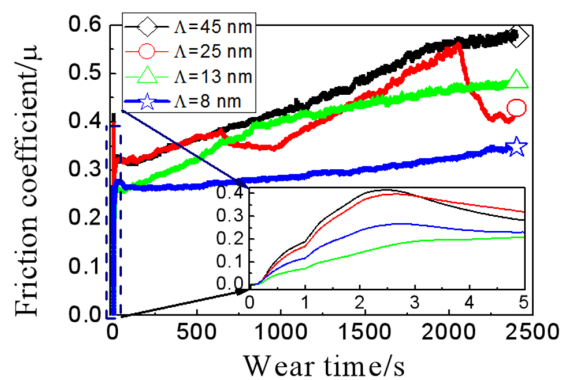

Figure 6. Calculated H/E and H^3/E^{*2} ratios of CrWN/MoN nano-multilayer coatings with different Λ.
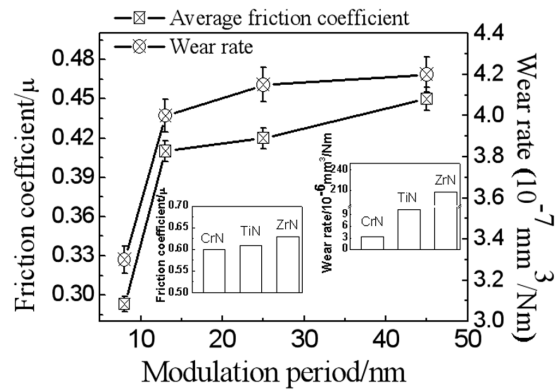

Figure 7. The friction coefficients and specific wear rates of CrWN/MoN nano-multilayer coatings with different modulation periods. The insets are the friction coefficients and wear rates of CrN [38], TiN [40] and ZrN [41] coatings.

Figure 8 shows the COF as a function of the wear time of CrWN/MoN nano-multilayer coatings with different Λ. It is noticeable that the CrWN/MoN coatings have short running-in times, as shown in the inset of Figure 8. Similar run-in stages mean that the surface of the coating has less influence on friction. The COF of CrWN/MoN nano-multilayer coatings increases with the increasing modulation period. At Λ = 13–45 nm, the COF increases gradually with the wear time. The COF at Λ = 8 nm is relatively stable with the wear time. The average COF and Wr of CrWN/MoN nano-multilayer coatings are presented in Figure 7. The average COF was obtained by averaging the real-time friction coefficient, which was

taken from 2/3 of the friction coefficients shown in Figure 8. The average COF increases from 0.29 to 0.45 as Λ increases from 8 nm to 45 nm. As for the specific Wr, an increase from 3.3×10^{-7} mm^3/Nm at Λ = 8 nm to 4.2×10^{-7} mm^3/Nm at Λ = 45 nm is observed. Wang [40] and Zhou [52] revealed that the wear properties of coatings are closely related to their H/E and H^3/E*^{2} values. In addition, the CrWN/MoN nano-multilayer coatings with higher Λ (13 nm, 25 nm and 45 nm) show a smooth wear morphology, while the coating with 8 nm Λ shows an abrasive wear morphology (as shown in Figure 9). Therefore, CrWN/MoN nano-multilayer coatings with different Λ show different mechanical properties and wear mechanisms, so the tribological properties of the coatings are different. Compared with the COF (0.6–0.7) and Wr ($3.3–207 \times 10^{-6}$ mm^3/Nm) of CrN [38], TiN [40] and ZrN [41], the wear resistance of CrWN/MoN nano-multilayer coatings is significantly improved. Compared with the COF (~0.5) and Wr (5×10^{-7} mm^3/Nm) of CrWN coatings, the wear resistance of CrWN/ MoN nano-multilayer coatings is also improved. Figure 10 shows the profiles of the wear tracks of the CrN monolayer coating, the CrWN monolayer coating and the CrWN/MoN nano-multilayer coating with 8 nm Λ. Under the same wear parameters, the CrWN/MoN nano-multilayer coating shows a wear depth of 0.2 µm, which is smaller than the wear depths of 0.25–0.35 µm for the CrN and CrWN monolayer coatings. The wear depth is obviously less than the thickness of the coating, which means that no substrate is exposed. The specific Wr of the coatings was calculated from the grooves of the wear tracks.

Figure 8. The friction coefficients of the CrWN/MoN nano-multilayer coatings with different modulation periods.
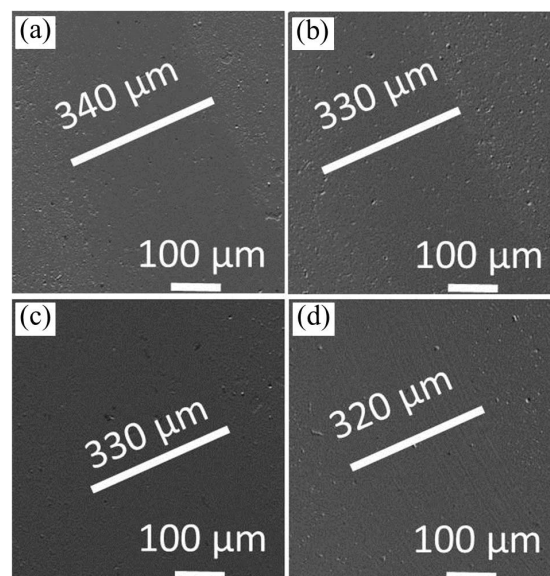
Figure 9. Wear morphologies of the CrWN/MoN nano-multilayer coatings with different modulation periods: (**a**) Λ = 45 nm, (**b**) Λ = 25 nm, (**c**) Λ = 13 nm, (**d**) Λ = 8 nm.
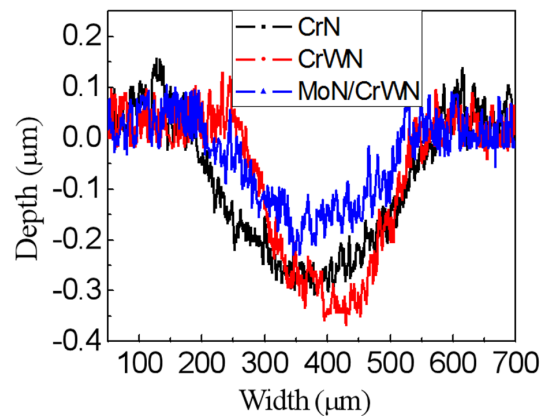
Figure 10. Profiles of wear tracks of CrN, CrWN and CrWN/MoN nano-multilayer coatings.

Figure 9 shows the wear morphologies of CrWN/MoN nano-multilayer coatings with different Λ from 8 nm to 45 nm. There are no tensile cracks of any type and/or spallation on the wear tracks of these coatings. The wear is slight, the wear surfaces are smooth, and there is no obvious debris at the edges of the wear tracks, but there are obvious pits and shallow furrows on the wear tracks. During the wear process, large particles fall off and form pits on the surface of wear. After large particles fall off, they are broken into small abrasive particles between the friction pair. Small abrasive particles play a pushing or cutting role in friction to form furrows on the wear track. The main wear mechanisms of CrN under dry friction are abrasive wear and adhesive wear [53,54], and there are a lot of debris and deep furrows at the edge of the wear track. MoN is introduced into CrWN coatings to form CrWN/MoN nano-multilayer coatings, and the wear mechanism is mild abrasive wear, which is evident from the wear morphology. During the friction process, tribochemical reactions may occur to form thin lubricating WO_3 and MoO_3 layers [55–57], which play the role of solid lubricants, significantly improve the wear resistance of the coating and reduce the damage degree of abrasive wear to the coatings, and only shallow furrows appear. At the same time, the nanometer multilayer structure improves the hardness of the coatings and also promotes the wear resistance of the coatings.

From the results of the study, compared with conventional monolayer coatings, it was found that the multilayer architectural design can provide improvements in mechanical and wear properties. With the variation in Λ, one sees a change in the mechanical and tribological properties of CrWN/MoN coatings. According to the Hall–Petch relationship, the hardness of coatings with 8 nm and 13 nm periods should be higher than that of coatings with 25 nm and 45 nm Λ. However, the coating with 13 nm Λ has the minimum hardness, which is lower than the hardness of coatings with 45 nm and 25 nm Λ, as shown in Figure 5. From Figure 4c, one sees a fuzzy non-coherent interface, which is different from the local coherent interface of the other Λ. The coherent interface can block the motion of dislocations, so compared with the coatings with coherent interfaces, we see the lower hardness of the coatings with non-coherent interfaces.

As shown in Figure 6, with the variation in Λ, the CrWN/MoN nano-multilayer coatings show different H/E and H^3/E^{*2} values. However, as shown in Figures 6–8, the tendencies of the tribological data of CrWN/MoN nano-multilayer coatings are consistent with the tendencies of hardness with varying Λ. It is presently accepted that the ratios of H/E and H^3/E^{*2} are important parameters for evaluating the tribological properties of hard coatings [47]. Coatings with higher H/E have better wear resistance [58]. It is clear that the best wear resistance is obtained from the hardest sample, with Λ = 8 nm, which has the lowest value of H/E. At Λ = 25 nm and 45 nm, the CrWN/MoN nano-multilayer coatings exhibit higher values of H/E, while the friction coefficients and wear rates are higher than those of the hardest sample with Λ = 8 nm. The results of the present study are in contrast to the understanding that higher H/E means better wear resistance. The results are consistent with the classical theories [59] that higher hardness means better

wear resistance. Archard's equation for abrasive wear shows that materials with higher hardness have better wear resistance [60]. The results of this work are consistent with results for graded Cr/CrN/CrTiN coatings [61], where the CrTiN-2A sample had the lowest H/E value with the best wear resistance. It was revealed that coatings with low elastic moduli and H/E > 0.1 have better crack resistance, which is useful for increasing wear resistance [62]. This refers to the redistribution of the load over a wider area, delaying the failure of the coating [37]. According to Beake et al. [63], in coatings with H/E < 0.1, the compatibility of hardness and toughness is easier to achieve in hard coatings. The combination of high hardness and a high H/E ratio of coatings is not conducive to anti-wear durability under high loads. In the present study, it is seen that the CrWN/MoN coating with Λ = 8 nm has the lowest H/E ratio, highest hardness and best wear resistance among all samples. According to references [61,64], wear resistance is not only related to the mechanical properties of the coatings but also affected by the stress state, wear mechanism and wear test condition of the coatings. The increase in hardness due to the macroscopic stress in the coatings is not beneficial for wear resistance improvement [49]. The study by Li et al. [65] shows that the friction coefficient and wear rate of MoS_2/Pb nanocomposite coatings under humid conditions (75% RH) are no longer in accord with the H/E values. In the process of the experiment, tribological tests were carried out with a large load (15 N) in a high-humidity environment (80%). This may be one reason for the friction coefficient and wear rate of the CrN/MoN coatings no longer matching the H/E value.

The interface plays a critical role in the coating's mechanical properties, which have an important effect on the tribological properties [8]. A multilayer structure is a useful way to obtain an interface between two different material layers. The interface depends on the modulation period and crystal structure. The interfaces of the multilayer coatings can be optimized by adjusting the modulation period, while the crystal structure also plays a role. The optimal properties of the multilayer CrWN/MoN coatings must be the result of multiple effects, such as the Hall–Petch relationship and dislocation blocking.

4. Conclusions

CrWN/MoN nano-multilayer coatings were prepared in pure N_2 by cathodic arc ion plating using CrW and Mo targets. The nano-multilayer structure is formed by the rotation of substrates. The influence of Λ on the microstructure, mechanical properties and wear resistance has been studied. The major conclusions are as follows:

(1) The CrWN/MoN nano-multilayer coatings consist of two phases: face-centered cubic CrWN and hexagonal δ-MoN. The nanoscale Λ and local coherent interfaces are confirmed by TEM and HRTEM.

(2) Λ has a significant effect on the hardness and wear properties of CrWN/MoN nano-multilayer coatings. With the variation in Λ, the hardness of CrWN/MoN nano-multilayer coatings changes from 25.5 GPa to 30.2 GPa, the average friction coefficient increases from 0.29 to 0.45, and the wear rate increases from 3.3×10^{-7} mm^3/Nm to 4.2×10^{-7} mm^3/Nm. Compared with monolayer coatings of CrN, TiN and ZrN, the mechanical and tribological properties of CrWN/MoN coatings are significantly improved by the nano-multilayer architecture.

(3) With increasing Λ, the interface shows different characteristics, and the values of H/E and H^3/E^{*2} ratios follow a similar evolutionary trend to that of the friction coefficient and wear rate. The interface has a critical influence on the coating properties. The combination of high hardness and low H/E is favorable for the wear resistance of CrWN/MoN nano-multilayer coatings, which is related to the hardness, the ratios of H/E and H^3/E^{*2}, and the wear mechanism.

Author Contributions: Conceptualization, Methodology, Writing—Review and Editing, C.T.; Visualization, Data Curation, Y.X.; Resources, Supervision, C.Z.; Visualization, Investigation, Y.Y.; Validation, T.A.; Review and editing, B.Y. and D.F. All authors have read and agreed to the published version of the manuscript.

Institutional Review Board Statement: Not applicable.

Informed Consent Statement: Not applicable.

Data Availability Statement: The data that support the findings of this study are available within the article.

Conflicts of Interest: The authors declare no conflict of interest.

References

1. Yao, S.H.; Su, Y.L.; Kao, W.H.; Cheng, K.W. Evaluation on wear behavior of Cr–Ag–N and Cr–W–N PVD nanocomposite coatings using two different types of tribometer. *Surf. Coat. Technol.* **2006**, *201*, 2520–2526. [CrossRef]
2. Jasempoor, F.; Elmkhah, H.; Imantalab, O.; Fattah-alhosseini, A. Improving the mechanical, tribological, and electrochemical behavior of AISI 304 stainless steel by applying CrN single layer and Cr/CrN multilayer coatings. *Wear* **2022**, *504–505*, 204425. [CrossRef]
3. Hauert, R.; Patscheider, J. From Alloying to Nanocomposites—Improved Performance of Hard Coatings. *Adv. Eng. Mater.* **2000**, *2*, 247–259. [CrossRef]
4. Ding, X.; Zeng, X.T.; Liu, Y.C.; Fang, F.Z.; Lim, G.C. Cr1−xAlxN coatings deposited by lateral rotating cathode arc for high speed machining applications. *Thin Solid Film.* **2008**, *516*, 1710–1715. [CrossRef]
5. Endrino, J.L.; Fox-Rabinovich, G.S.; Reiter, A.; Veldhuis, S.V.; Escobar Galindo, R.; Albella, J.M.; Marco, J.F. Oxidation tuning in AlCrN coatings. *Surf. Coat. Technol.* **2007**, *201*, 4505–4511. [CrossRef]
6. Lin, J.; Wang, B.; Ou, Y.; Sproul, W.D.; Dahan, I.; Moore, J.J. Structure and properties of CrSiN nanocomposite coatings deposited by hybrid modulated pulsed power and pulsed dc magnetron sputtering. *Surf. Coat. Technol.* **2013**, *216*, 251–258. [CrossRef]
7. Zhang, S.; Li, J.; Tu, R.; Ando, K.; Gao, T. Improved hardness of semi-coherent TiN/CrN nano-multilayer coating through manipulation of structure evolution. *Mater. Sci. Eng. A* **2023**, *886*, 145728. [CrossRef]
8. Xu, Y.X.; Chen, L.; Pei, F.; Du, Y. Structure and thermal properties of TiAlN/CrN multilayered coatings with various modulation ratios. *Surf. Coat. Technol.* **2016**, *304*, 512–518. [CrossRef]
9. Subramanian, C.; Strafford, K.N. Review of multicomponent and multilayer coatings for tribological applications. *Wear* **1993**, *165*, 85–95. [CrossRef]
10. Liang, B.-H.; Hsieu, F.-S.; Wu, F.-B. Modulation effect on mechanical properties of nanolayered MoN/MoSiN coatings. *Surf. Coat. Technol.* **2022**, *436*, 128278. [CrossRef]
11. Anderson, P.M.; Li, C. Hall-Petch relations for multilayered materials. *Nanostruct. Mater.* **1995**, *5*, 349–362. [CrossRef]
12. Sproul, W.D. Reactive sputter deposition of polycrystalline nitride and oxide superlattice coatings. *Surf. Coat. Technol.* **1996**, *86–87*, 170–176. [CrossRef]
13. Sundgren, J.E.; Birch, J.; Håkansson, G.; Hultman, L.; Helmersson, U. Helmersson Growth, Structural Charaterization and Properties of Hard and Wear-protective Layered Materials. *Thin Solid Film.* **1990**, *193–194*, 818–831. [CrossRef]
14. Xu, Y.X.; Chen, L.; Pei, F.; Chang, K.K.; Du, Y. Effect of the modulation ratio on the interface structure of TiAlN/TiN and TiAlN/ZrN multilayers: First-principles and experimental investigations. *Acta Mater.* **2017**, *130*, 281–288. [CrossRef]
15. Helmersson, U.; Todorova, S.; Barnett, S.A.; Sundgren, J.-E.; Markert, L.C.; Greene, J.E. Growth of single-crystal TiN/VN strained-layer superlattices with extremely high mechanical hardness. *J. Appl. Phys.* **1987**, *62*, 481–484. [CrossRef]
16. Kim, S.H.; Baik, Y.J.; Kwon, D. Analysis of interfacial strengthening from composite hardness of TiN/VN and TiN/NbN multilayer hard coatings. *Surf. Coat. Technol.* **2004**, *187*, 47–53. [CrossRef]
17. Hones, P.; Diserens, M.; Sanjinés, R.; Lévy, F. Electronic structure and mechanical properties of hard coatings from the chromium–tungsten nitride system. *J. Vac. Sci. Technol. B Microelectron. Nanometer Struct. Process. Meas. Phenom.* **2000**, *18*, 2851–2856. [CrossRef]
18. Yau, B.-S.; Chu, C.-W.; Lin, D.; Lee, W.; Duh, J.-G.; Lin, C.-H. Tungsten doped chromium nitride coatings. *Thin Solid Film.* **2008**, *516*, 1877–1882. [CrossRef]
19. Lin, C.-H.; Duh, J.-G.; Yau, B.-S. Processing of chromium tungsten nitride hard coatings for glass molding. *Surf. Coat. Technol.* **2006**, *201*, 1316–1322. [CrossRef]
20. Mei, H.; Zhao, S.; Wu, Z.; Dai, W.; Wang, Q. Effect of nitrogen partial pressure on microstructure and mechanical properties of Mo-Cu-V-N composite coatings deposited by HIPIMS. *Surf. Coat. Technol.* **2017**, *329*, 68–76. [CrossRef]
21. Heo, S.J.; Kim, K.H.; Kang, M.C.; Suh, J.H.; Park, C.-G. Syntheses and mechanical properties of Mo–Si–N coatings by a hybrid coating system. *Surf. Coat. Technol.* **2006**, *201*, 4180–4184. [CrossRef]

22. Wang, T.; Zhang, J.; Li, Y.; Gao, F.; Zhang, G. Self-lubricating TiN/MoN and TiAlN/MoN nano-multilayer coatings for drilling of austenitic stainless steel. *Ceram. Int.* **2019**, *45*, 24248–24253. [CrossRef]

23. Postolnyi, B.O.; Beresnev, V.M.; Abadias, G.; Bondar, O.V.; Rebouta, L.; Araujo, J.P.; Pogrebnjak, A.D. Multilayer design of CrN/MoN protective coatings for enhanced hardness and toughness. *J. Alloys Compd.* **2017**, *725*, 1188–1198. [CrossRef]

24. Pogrebnjak, A.D.; Beresnev, V.M.; Bondar, O.V.; Postolnyi, B.O.; Zaleski, K.; Coy, E.; Jurga, S.; Lisovenko, M.O.; Konarski, P.; Rebouta, L.; et al. Superhard CrN/MoN coatings with multilayer architecture. *Mater. Des.* **2018**, *153*, 47–59. [CrossRef]

25. Maksakova, O.V.; Simoẽs, S.; Pogrebnjak, A.D.; Bondar, O.V.; Kravchenko, Y.O.; Koltunowicz, T.N.; Shaimardanov, Z.K. Multilay-ered ZrN/CrN coatings with enhanced thermal and mechanical properties. *J. Alloys Compd.* **2019**, *776*, 679–690. [CrossRef]

26. Wu, F.-B.; Tien, S.-K.; Duh, J.-G. Manufacture, microstructure and mechanical properties of CrWN and CrN/WN nanolayered coatings. *Surf. Coat. Technol.* **2005**, *200*, 1514–1518. [CrossRef]

27. Shan, L.; Zhang, Y.; Wang, Y.; Li, J.; Jiang, X.; Chen, J. Corrosion and wear behaviors of PVD CrN and CrSiN coatings in seawater. *Trans. Nonferrous Met. Soc. China* **2016**, *26*, 175–184. [CrossRef]

28. Gilewicz, A.; Warcholinski, B.; Murzynski, D. The properties of molybdenum nitride coatings obtained by cathodic arc evaporation. *Surf. Coat. Technol.* **2013**, *236*, 149–158. [CrossRef]

29. Kravchenko, Y.O.; Coy, L.E.; Peplińska, B.; Iatsunskyi, I.; Załeski, K.; Kempiński, M.; Beresnev, V.M.; Konarski, P.; Jurga, S.; Pogrebnjak, A.D. Nano-multilayered coatings of (TiAlSiY)N/MeN (Me=Mo, Cr and Zr): Influence of composition of the alternating layer on their structural and mechanical properties. *J. Alloys Compd.* **2018**, *767*, 483–495. [CrossRef]

30. Nemchinsky, V. Modeling Arc in Transverse Magnetic Field by Using Minimum Principle. *IEEE Trans. Plasma Sci.* **2016**, *44*, 2932–2935. [CrossRef]

31. Takikawa, H.; Tanoue, H. Review of Cathodic Arc Deposition for Preparing Droplet-Free Thin Films. *IEEE Trans. Plasma Sci.* **2007**, *35*, 992–999. [CrossRef]

32. Krysina, O.V.; Ivanov, Y.F.; Koval, N.N.; Prokopenko, N.A.; Shugurov, V.V.; Petrikova, E.A.; Tolkachev, O.S. Composition, structure and properties of Mo-N coatings formed by the method of vacuum-arc plasma-assisted deposition. *Surf. Coat. Technol.* **2021**, *416*, 127153. [CrossRef]

33. Zhou, Z.; Rainforth, W.M.; Rother, B.; Ehiasarian, A.P.; Hovsepian, P.E.; Münz, W.-D. Elemental distributions and substrate rotation in industrial TiAlN/VN superlattice hard PVD coatings. *Surf. Coat. Technol.* **2004**, *183*, 275–282. [CrossRef]

34. Voevodin, A.A.; Zabinski, J.S.; Muratore, C. Recent advances in hard, tough, and low friction nanocomposite coatings. *Tsinghua Sci. Technol.* **2005**, *10*, 665–679. [CrossRef]

35. Setoyama, M.; Nakayama, A.; Tanaka, M.; Kitagawa, N.; Nomura, T. Formation of cubic-AIN in TiN/AIN superlattice. *Surf. Coat. Technol.* **1996**, *86-87*, 225–230. [CrossRef]

36. Shinn, M.; Barnett, S.A. Effect of superlattice layer elastic moduli on hardness. *Appl. Phys. Lett.* **1994**, *64*, 61–63. [CrossRef]

37. Zhou, S.Y.; Yan, S.J.; Han, B.; Yang, B.; Lin, B.Z.; Zhang, Z.D.; Ai, Z.W.; Pelenovich, V.O.; Fu, D.J. Influence of modulation period and modulation ratio on structure and mechanical properties of TiBN/CrN coatings deposited by multi-arc ion plating. *Appl. Surf. Sci.* **2015**, *351*, 1116–1121. [CrossRef]

38. Tian, C.X.; Han, B.; Zou, C.W.; Xie, X.; Li, S.Q.; Liang, F.; Tang, X.S.; Wang, Z.S.; Pelenovich, V.O.; Zeng, X.M.; et al. Synthesis of monolayer MoNx and nanomultilayer CrN/Mo2N coatings using arc ion plating. *Surf. Coat. Technol.* **2019**, *370*, 125–129. [CrossRef]

39. He, S.; Lu, H.; Tian, C.; Liu, Y.; Li, Z. Influence of N2 pressure on the microstructure and properties of CrWN coatings. *Mater. Sci. Eng. Powder Metall.* **2021**, *26*, 235–242.

40. Wang, Y.H.; Guo, F.; Ren, H.; Hu, S.Y.; Chen, Y.J.; Zhao, Y.H.; Gong, F.; Xie, Z.W. Enhancing wear resistance of TiN coating by gradient bias voltage and arc-enhanced glow discharge. *Ceram. Int.* **2022**, *48*, 8746–8750. [CrossRef]

41. Krysina, O.V.; Ivanov, Y.F.; Prokopenko, N.A.; Shugurov, V.V.; Petrikova, E.A.; Denisova, Y.A.; Tolkachev, O.S. Influence of Nb addition on the structure, composition and properties of single-layered ZrN-based coatings obtained by vacuum-arc deposition method. *Surf. Coat. Technol.* **2020**, *387*, 125555. [CrossRef]

42. Mayrhofer, P.H.; Mitterer, C.; Hultman, L.; Clemens, H. Microstructural design of hard coatings. *Prog. Mater. Sci.* **2006**, *51*, 1032–1114. [CrossRef]

43. Stueber, M.; Holleck, H.; Leiste, H.; Seemann, K.; Ulrich, S.; Ziebert, C. Concepts for the design of advanced nanoscale PVD multilayer protective thin films. *J. Alloys Compd.* **2009**, *483*, 321–333. [CrossRef]

44. Sun, Y.D.; Tan, M.; Gong, J.; Liu, M.Y.; Liu, G.Q.; Deng, X.Y.; Li, D.J. Effect of Modulation Period and N+Beam Bombarding Energy on the growth of Nanoscale ZrB2/AlN Multilayered Coatings Prepared by IBAD. *Phys. Procedia* **2011**, *18*, 154–159. [CrossRef]

45. Chen, L.; Xu, Y.X.; Zhang, L.J. Influence of TiN and ZrN insertion layers on the microstructure, mechanical and thermal properties of Cr–Al–N coatings. *Surf. Coat. Technol.* **2016**, *285*, 146–152. [CrossRef]

46. Yalamanchili, K.; Wang, F.; Aboulfadl, H.; Barrirero, J.; Rogström, L.; Jiménez-Pique, E.; Mücklich, F.; Tasnadi, F.; Odén, M.; Ghafoor, N. Growth and thermal stability of TiN/ZrAlN: Effect of internal interfaces. *Acta Mater.* **2016**, *121*, 396–406. [CrossRef]

47. Pogrebnjak, A.; Smyrnova, K.; Bondar, O. Nanocomposite Multilayer Binary Nitride Coatings Based on Transition and Refractory Metals: Structure and Properties. *Coatings* **2019**, *9*, 155. [CrossRef]

48. Ou, Y.X.; Lin, J.; Che, H.L.; Moore, J.J.; Sproul, W.D.; Lei, M.K. Mechanical and tribological properties of CrN/TiN superlattice coatings deposited by a combination of arc-free deep oscillation magnetron sputtering with pulsed dc magnetron sputtering. *Thin Solid Film.* **2015**, *594*, 147–155. [CrossRef]

49. Philippon, D.; Godinho, V.; Nagy, P.M.; Delplancke-Ogletree, M.P.; Fernández, A. Endurance of TiAlSiN coatings: Effect of Si and bias on wear and adhesion. *Wear* **2011**, *270*, 541–549. [CrossRef]

50. Liu, H.; Yang, F.-C.; Tsai, Y.-J.; Wang, X.; Li, W.; Chang, C.-L. Effect of modulation structure on the microstructural and mechanical properties of TiAlSiN/CrN thin films prepared by high power impulse magnetron sputtering. *Surf. Coat. Technol.* **2019**, *358*, 577–585. [CrossRef]

51. Musil, J.; Jirout, M. Toughness of hard nanostructured ceramic thin films. *Surf. Coat. Technol.* **2007**, *201*, 5148–5152. [CrossRef]

52. Zhou, S.Y.; Pelenovich, V.O.; Han, B.; Yousaf, M.I.; Yan, S.J.; Tian, C.X.; Fu, D.J. Effects of modulation period on microstructure, mechanical properties of TiBN/TiN nanomultilayered films deposited by multi arc ion plating. *Vacuum* **2016**, *126*, 34–40. [CrossRef]

53. Li, Z.; Guan, X.; Wang, Y.; Li, J.; Cheng, X.; Lu, X.; Wang, L.; Xue, Q. Comparative study on the load carrying capacities of DLC, GLC and CrN coatings under sliding-friction condition in different environments. *Surf. Coat. Technol.* **2017**, *321*, 350–357. [CrossRef]

54. Teng, Y.; Guo, Y.-Y.; Zhang, M.; Yang, Y.-J.; Huang, Z.; Zhou, Y.-W.; Wu, F.-Y.; Liang, Y.-S. Effect of Cr/CrNx transition layer on mechanical properties of CrN coatings deposited on plasma nitrided austenitic stainless steel. *Surf. Coat. Technol.* **2019**, *367*, 100–107. [CrossRef]

55. Huang, X.; Xie, Z.; Li, K.; Chen, Q.; Gong, F.; Chen, Y.; Feng, B.; Hu, S.; Chen, Y.; Han, B.; et al. Microstructure, wear and oxidation resistance of CrWN glass molding coatings synthesized by plasma enhanced magnetron sputtering. *Vacuum* **2020**, *174*, 109206. [CrossRef]

56. Choi, E.Y.; Kang, M.C.; Kwon, D.H.; Shin, D.W.; Kim, K.H. Comparative studies on microstructure and mechanical properties of CrN, Cr–C–N and Cr–Mo–N coatings. *J. Mater. Process. Technol.* **2007**, *187–188*, 566–570. [CrossRef]

57. Roy, A.; Patel, P.; Sharifi, N.; Chromik, R.R.; Stoyanov, P.; Moreau, C. Binary and ternary lubricious oxides for high temperature tribological applications: A review. *Results Surf. Interfaces* **2023**, *11*, 100117. [CrossRef]

58. Leyland, A.; Matthews, A. On the significance of the H/E ratio in wear control: A nanocomposite coating approach to optimised tribological behaviour. *Wear* **2000**, *246*, 1–11. [CrossRef]

59. Archard, J.F. Contact and Rubbing of Flat Surfaces. *J. Appl. Phys.* **1953**, *24*, 981–988. [CrossRef]

60. Hutchings, I. *Tribology: Friction and Wear of Engineering Materials*; Materials Research Society symposium proceedings; Hutchings, I.M., Ed.; CRC: Boca Raton, FL, USA, 1992; ISBN 034056184.

61. Kabir, M.S.; Munroe, P.; Zhou, Z.; Xie, Z. Scratch adhesion and tribological behaviour of graded Cr/CrN/CrTiN coatings synthesized by closed-field unbalanced magnetron sputtering. *Wear* **2017**, *380–381*, 163–175. [CrossRef]

62. Musil, J. Hard nanocomposite coatings: Thermal stability, oxidation resistance and toughness. *Surf. Coat. Technol.* **2012**, *207*, 50–65. [CrossRef]

63. Beake, B.D.; Vishnyakov, V.M.; Harris, A.J. Relationship between mechanical properties of thin nitride-based films and their behaviour in nano-scratch tests. *Tribol. Int.* **2011**, *44*, 468–475. [CrossRef]

64. Ni, W.; Cheng, Y.-T.; Lukitsch, M.J.; Weiner, A.M.; Lev, L.C.; Grummon, D.S. Effects of the ratio of hardness to Young's modulus on the friction and wear behavior of bilayer coatings. *Appl. Phys. Lett.* **2004**, *85*, 4028–4030. [CrossRef]

65. Li, H.; Zhang, G.; Wang, L. Low humidity-sensitivity of MoS2/Pb nanocomposite coatings. *Wear* **2016**, *350–351*, 1–9. [CrossRef]